Spatial integration of fry and fractal analyses in regional exploration: A case study from Bafq–Posht-e-Badam, Irán

Integración espacial de los análisis fry y fractal para la exploración regional: Un estudio de caso en Bafq-Posht-e-Badam, Irán

Ali Najafi[1, 2*], Maryam Abdi[1], Behnam Rahimi[1] & Kamran Motevali[2]
[1]Department of Geology, Ferdowsi University of Mashhad, Mashhad, Islamic Republic of Iran
[2]National Geoscience Database of Iran
[*]Corresponding author, a.najafi@stu-mail.um.ac.ir

Najafi, Ali; Abdi, Maryam; Rahimi, Behnam & Motevali, Kamran (2010): Spatial Integration of Fry and Fractal Analyses in Regional Exploration: A Case Study from Bafq–Posht-e-Badam, Iran [*Integración Espacial de los análisis Fry y Fractal para la Exploración regional: Un Estudio de Caso en Bafq-Posht-e-Badam, Irán*]. Geología Colombiana, Vol. 35. pp 113-130. Bogotá, Colombia.

Artículo de Investigación Cientifica Manuscrito recibido: 2 de mayo de 2010; aceptado: 21 de agosto de 2010

Abstract

This research examines the fractal and fry analysis which are implemented as complementary methods to evaluate their efficiency as regional exploration tools. The disadvantage of the "Box-counting" method lies in its inadequacy in dealing with low numbers of point data sets. Attempts have been made to use spatial integration of airborne geophysical data to turn this method into a useful tool for detecting mineral occurences.

According to the mineralization trends, results from Fry analysis using the rose diagram of the faults within the area, have confirmed field observations concerning structurally controlled mineral occurences. This suggests that the fractal dimension in the 'Box-counting' method must be similar for both mineralization points and fault lines, but that is not the case for the study area. Furthermore, the 'number-in-circle' method has been applied to check the anomaly points, whose fractal dimension corresponds to that of the fault lines in the 'Box-counting' method. The difference between fractal dimensions of mineralization points and those of fault systems lies in the low number of recognized occurrences. This issue can serve as an exploration key in leading to some promising areas that need more complementary research, as well as underground survey. The significance of airborne geophysical survey in iron deposits mapping and prospecting is in providing valuable information for a better understanding of the spatial pattern of mineralization as well as in showing exploration targets within new high-priority areas, and in providing a useful technique to develop spatial data modeling for regional exploration.

Keywords: Fry, fractal, airborne geophysics, spatial integration, regional exploration, Iran

Resumen

Los análisis fry y fractales se usan como métodos complementarios para evaluar la eficacia de las herramientas de exploración regional. La desventaja del método "Box counting" radica en su insuficiencia para usar pocos números en conjuntos de datos tipo punto. Se han hecho intentos para utilizar la integración espacial de datos geofísicos aéreos en la transformación de este método, a fin de convertirlo en una herramienta útil para detectar mineralizaciones.

Según las tendencias de mineralización, los resultados procedentes del análisis fry, utilizando diagramas rosa, para las fracturas dentro del área de estudio, confirman observaciones de campo acerca de ocurrencias minerales controladas estructuralmente. Esto sugiere que la dimensión fractal del método "box counting" debe ser similar, tanto en los puntos de mineralización, como en las líneas de fallas, pero este no es el caso de la zona de estudio. Además, el método "number-in-circle" ha sido aplicado para chequear los puntos de anomalía, cuya dimensión fractal corresponde a la de las líneas de fractura en el método "box counting". La diferencia entre dimensiones fractales de puntos de mineralización y aquellas de los sistemas de fallas se explica por el bajo número de

ocurrencias reconocidas. Esto puede servir como clave de exploración para aquellas zonas mineralizadas que requieren investigación complementaria, así como en la exploración subterránea. La importancia del estudio geofísico aéreo durante el mapeo y la prospección de depósitos de hierro radica en que puede proveer información valiosa para una mejor comprensión del patrón espacial de la mineralización, así como para señalar objetivos de exploración dentro de nuevas áreas de alta prioridad. Puede, adicionalmente, convertirse en una técnica de utilidad para desarrollar modelos de datos espaciales aplicados a la exploración regional.

Palabras clave: Fry, fractales, geofísica aérea, integración espacial, exploración regional, Irán.

Introduction

Advances in the manipulation of large and diverse data sets have enabled experts in mineral exploration to increasingly utilize computer-based and conceptual strategies that can significantly enhance a field-based empirical approach (Bierlein *et al.,* 2006). This has led to the development of a variety of techniques, using knowledge-driven and/or data-driven approaches, to extract exploration-related factors efficiently from multi-disciplinary data sets that can be integrated into mineral favorability maps at various geographical scales (Bonham-Carter, 1994; Bierlein *et al*., 2006). The spatial distribution of mineral deposits is a concern in regional exploration and assessment of undiscovered resources (Vearncombe & Vearncombe, 1999). There are different methods of spatial analysis that reveal spatial distribution patterns of mineral deposit occurrences. Two appropriate methods are Fractal and Fry analyses. Fry analysis can be used as a complementary method for Fractal analysis when we deal with point data sets such as mineral deposit occurrences.

Regional Geology

The study area comprises 15000 km^2 in Central Iran and is covered by six 1:100 000 scale maps that include the Zamanabad, Saghand, Chadormalou, Ariz, Esfordi and Bafq quadrangles (Fig. 1).

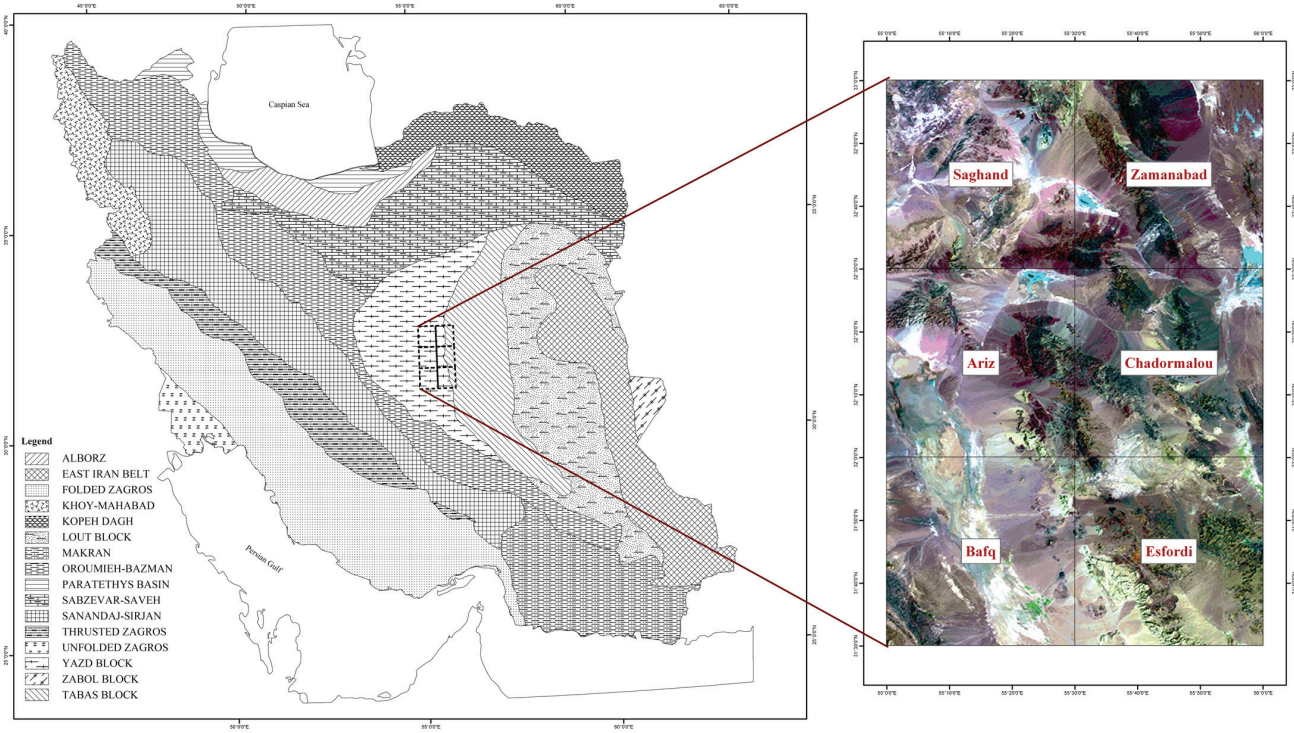

Figure 1. Simplified sedimentary structural units of Irán and location of the study area are compiled from Berberian & King (1981), Eftekharnejad (1981), Alavi (1991), Aghanabati (2002) and include six 1:100 000 scale maps of Zamanabad, Saghand, Chadormalou, Ariz, Esfordi and Bafq quadrangles.

Tectonically, the Bafq–Posht-e-Badam mining district is in the Kashmar-Kerman volcano-plutonic arcuate zone, which is in turn part of the Central Iranian zone that hosts important Kiruna-type magnetite-apatite deposits (Torab & Lehmann, 2007). This district is bordered by three major fault zones: The Posht-e- Badam Fault to the west, the Kuh-Banan and the Kalmard faults to the east. Stratigraphic divisions in Central Irán generally can be temporally divided into three units: Neoproterozoic, Cambrian and younger sequences (Jami, 2005). Late Neoproterozoic metamorphosed sequences in Central Irán are divided into four lithostratigraphic units: Earlier Series, Chapedony Complex, Bonehshuro Complex and Tashk Formation (Haghipour, 1964).

The Tashk Formation in the study area contains high-to-low-grade metamorphic rocks such as schist, gneiss, amphibolite, quartzite and marble (comprising the Boneh-Shurow and Sarkuh Complexes) as well as low-grade salty shale, quartzitic sandstone, greywacke and phyllite. These orogenic sequences are unconformably underlain by an Early Cambrian high-K calc-alkaline volcano-sedimentary sequence called the Esfordi Formation, which mainly consists of dolomite and volcanic rocks. This sequence has been also termed the Rizu-Dezu Series or the Saghand Formation in different parts of the area by different researchers (Haghipour, 1964; Forster & Jafarzadeh, 1994; Samani, 1988; Daliran, 1999; Jami, 2005). U-Pb dating of zircon from rhyolitic units of these volcano-sedimentary rocks yielded ages of 529 to 554 Ma (Ramezani & Tucker, 2003). The metamorphic and volcano-sedimentary sequences are intruded by cambrian plutonic rocks, with compositions from granite to granodiorite and gabbro-diorite and with a calc-alkaline signature (Torab & Lehmann, 2007). The plutonic rocks in the Saghand area are 525 to 533 Ma (Ramezani & Tucker, 2003). The Fe-oxide–apatite ores and apatites are spatially and temporally associated with the volcano-sedimentary unit (Daliran, 1999). A simplified geologic map is presented in Fig. 2.

Considering magmatism and sedimentation in the study area, an anorogenic intra-continental rifting model along the Proto-Tethyan margin of Gondwana has been proposed (Daliran, 2002). It should be mentioned that the existence of rift zones in the Bafq district are associated with spilitic basalts and regional alkali metasomatism, along with the development of evaporite facies within the volcano-sedimentary units; all this suggest the establishment of an extensional regime in this region that is probably genetically related to the mineralization (Daliran & Stosch, 2007).

Mineralization proccesses in the field

The Bafq–Posht-e-Badam mining district is the most important iron realated metallogenic province in Iran. It includes more than 80 iron deposits ranging in size up to more than 400 m in some large mines such as Chador-Malu which, considering associated magnetic anomalies, encompass a wide variety of mineral occurrences (Martin *et al.,* 1998; Jami, 2005). The origin of the iron-oxide deposits has long been controversial and various genetic models have been suggested (Torab & Lehmann, 2007). Some researchers believe in magmatic origins (Frietsch, 1978; Nystrom & Henriquez, 1994, Naslund *et al.,* 2002), while others suggest the exhalative-synsedimentary (Torab & Lehmann, 2007) or epigenetic-hydrothermal models (Bookstrom, 1977; Hildebrand, 1986; Gleason *et al.*, 2000; Sillitoe & Burrows, 2002; Torab & Lehmann, 2007). Current studies consider all the previously-known Kiruna-type deposits belonging to the hydrothermal iron-oxide-copper-gold (IOCG) clans (Hitzman *et al.,* 1992; Barton & Johnson, 1996; 2000; Hitzman, 2000). These types of deposits are thought to be related to large scale faults that aid to the development of intense metasomatic replacement (Samani, 1998; Daliran, 1999; Torab & Lehmann, 2007). The geologic setting of these deposits is either a rifted continental margin (back arcs) or an intercontinental rift (anorogenic) within a sub-aerial to shallow marine basin sequence (Hitzman, 2000; Torab & Lehmann, 2007).

Methodology and data sets

The location of 81 mineral sites (Tab. 1), reported in several publications (Jami, 2005; NISCO 1969, 1971, 1974, 1975, 1979a, 1979b, 1980), were used in this study to obtain a general view of the spatial pattern of mineral occurrences in the area.

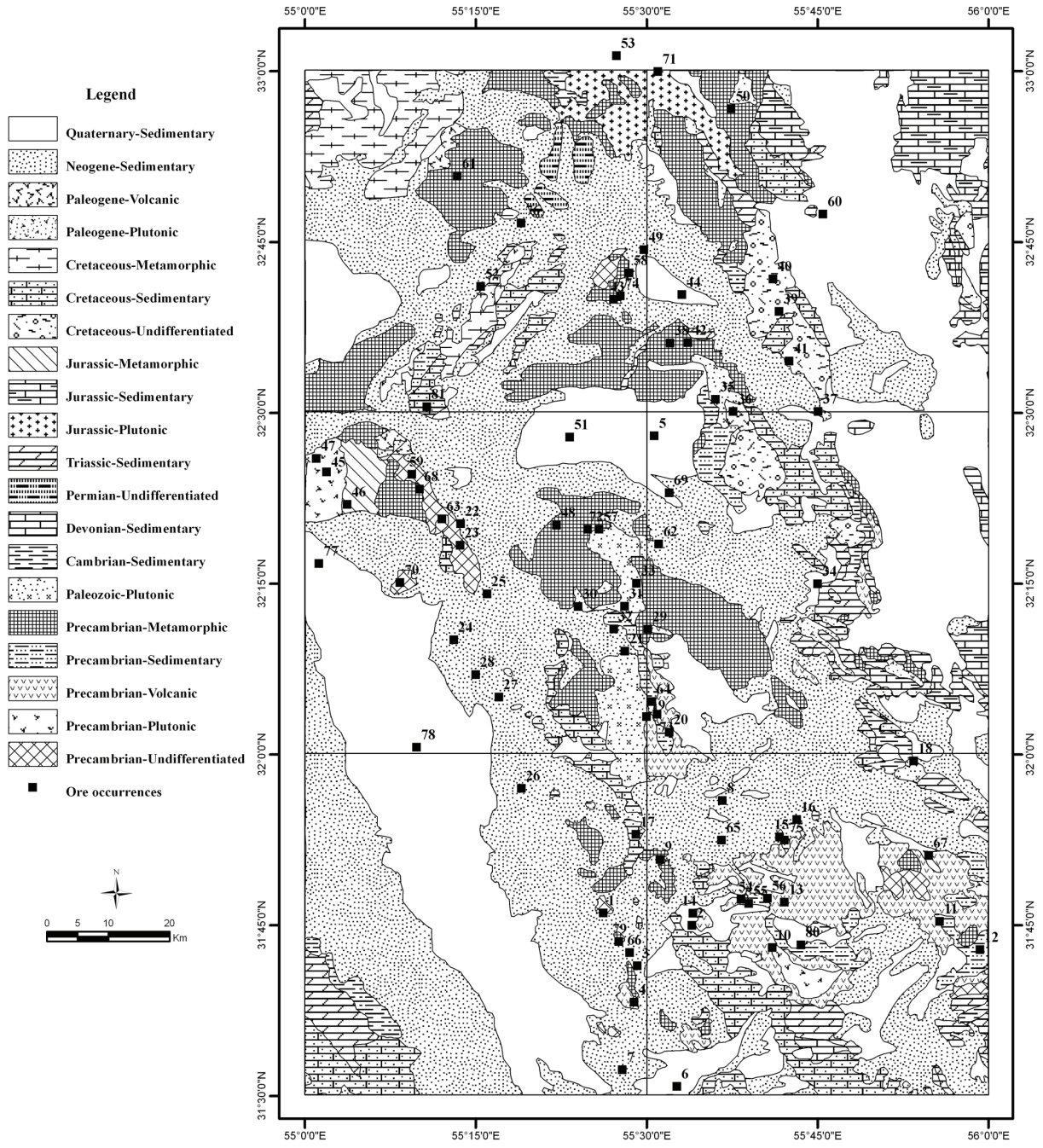

Figure 2. Simplified regional geologic map of the Bafq–Posht-e-Badam District, including mineral occurrences. Modified from six 1:100 000 scale maps: (Soheili & Mahdavi, 1991; Babakhani & Ghalamghash, 1999; Babakhani & Majidi 1995, Majidi & Babakhani 2000; Amini *et al.,* 2004; Ghaemi & Saidi, 2006) and three 1:250 000 scale maps: (Valeh & Haghipour, 1970; Nabavi 1972; Mahdavi, 1996)

Table 1. Latitude and longitude of iron resources within the study area.

No.	Name	X	Y	No.	Name	X	Y	No.	Name	X	Y
1	IA	55.436667	31.768333	28	XVIIA	55.400000	32.216667	55	Esfordi 2	55.649444	31.782222
2	IC	55.566667	31.750000	29	XVIIB	55.468056	32.217222	56	Esfordi 3	55.676944	31.790000
3	ID	55.486667	31.691111	30	XVIIC	55.452222	32.184167	57	Poshte Sorkh	55.430556	32.330000
4	IIA	55.481944	31.637778	31	XVIIIB	55.485556	32.250833	58	Gelmandeh	55.474444	32.705000
5	IIB	55.511389	32.466667	32	XVIIIC	55.750556	32.250000	59	Sorkhou	55.156667	32.410278
6	IIC	55.544444	31.514722	33	XXA	55.601111	32.520278	60	Jahanshir	55.758333	32.791111
7	III	55.464722	31.538889	34	XXB	55.626944	32.502222	61	Chapedoni	55.223333	32.846944
8	IV	55.611111	31.932778	35	XXC	55.751389	32.502222	62	Chadormalou	55.518056	32.308333
9	IX	55.520000	31.846667	36	XXIA	55.693889	32.648611	63	Chah Jamal	55.200556	32.345278
10	VB	55.928889	31.755833	37	XXI-A	55.534444	32.602500	64	Chah Gaz	55.507778	32.077778
11	VC	55.988056	31.714722	38	XXIB	55.685000	32.696111	65	Cheshmeh Firouz	55.610000	31.875000
12	VIII	55.568056	31.768056	39	XXIC	55.708889	32.576111	66	Choghart	55.475556	31.710556
13	X	55.694722	31.879444	40	XXII-B	55.560833	32.603333	67	East Bafq	55.913056	31.852500
14	XI	55.720000	31.905278	41	XXIII-A	55.451667	32.666667	68	Khoshoumi	55.167778	32.388889
15	XIIB	55.484722	31.883611	42	XXIII-B	55.551944	32.673611	69	Douzakh Dareh	55.533333	32.383333
16	XIIIA	55.891111	31.990833	43	XXIV-A	55.031944	32.413889	70	Dig Dome Khomar	55.139444	32.251944
17	XIIIB	55.500000	32.055833	44	XXIV-B	55.061944	32.366389	71	Robat Posht Badam	55.516667	33.000000
18	XIIIC	55.533333	32.032778	45	XXIV-C	55.016944	32.433611	72	Zaj Poshte Sorkh	55.414167	32.330000
19	XIVD	55.468611	32.151389	46	XXTX	55.368333	32.335833	73	Zarigan	55.515556	32.059167
20	XIXA	55.228333	32.338056	47	XXV	55.496111	32.739167	74	Zaman Abad	55.461944	32.671667
21	XIXB	55.227500	32.306389	48	XXVI	55.623889	32.945556	75	Se Chahoun	55.701944	31.875000
22	XIXC	55.218056	32.168056	49	XXX	55.387778	32.464722	76	North Allah Abad	55.316667	32.778056
23	XIXD	55.266667	32.235556	50	XXXII	55.257500	32.685278	77	Fakhr Abad	55.020833	32.280000
24	XV	55.316944	31.950556	51	XXXIII	55.456111	33.023056	78	Moghestan	55.163611	32.011111
25	XVIA	55.284167	32.084167	52	Ashitusa	55.683889	31.717778	79	Mishdovan	55.459444	31.726667
26	XVIB	55.250000	32.117222	53	Lakeh Siah	55.701944	31.784167	80	Narigan	55.726111	31.721667
27	XVID	55.502222	32.183611	54	Esfordi 1	55.638611	31.788611	81	Neybaz	55.178611	32.509167

The exploration data indicate that the iron mineralization can generally be classified into three styles: ore occurrences, mineral deposits and mines. Thus, we considered these data under separate categories to obtain a general insight into their spatial patterns. Fry analysis has been applied to reveal the main trends of mineralization. The deposit data have been classified into five classes (Tab. 2) and the points for each class have been horizontally translated by following the procedure described by Vearncombe & Vearncombe (1999).

Rose diagrams of trends among translated points were constructed to describe the spatial distribution pattern (Fig. 3, Tab. 3).

Table 2. Classification of iron ore occurrence in the study area into 5 classes

ID	Class	Number of ore occurrence	Number of Translations points
A	Total ore occurrence in whole	81	6480
B	Ore indications in whole of	30	870
C	Mineral deposits and mines in	51	2550
D	Ore occurrence in north part of	34	1122
E	Ore occurrence in south part of	47	2162

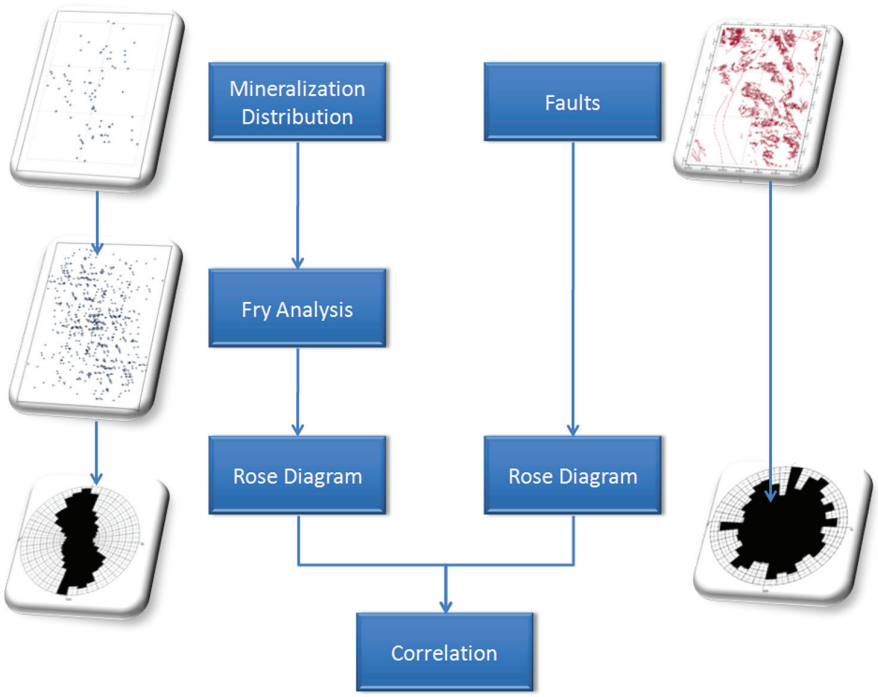

Figure 3. Schematic diagram showing the stagewise fry analysis

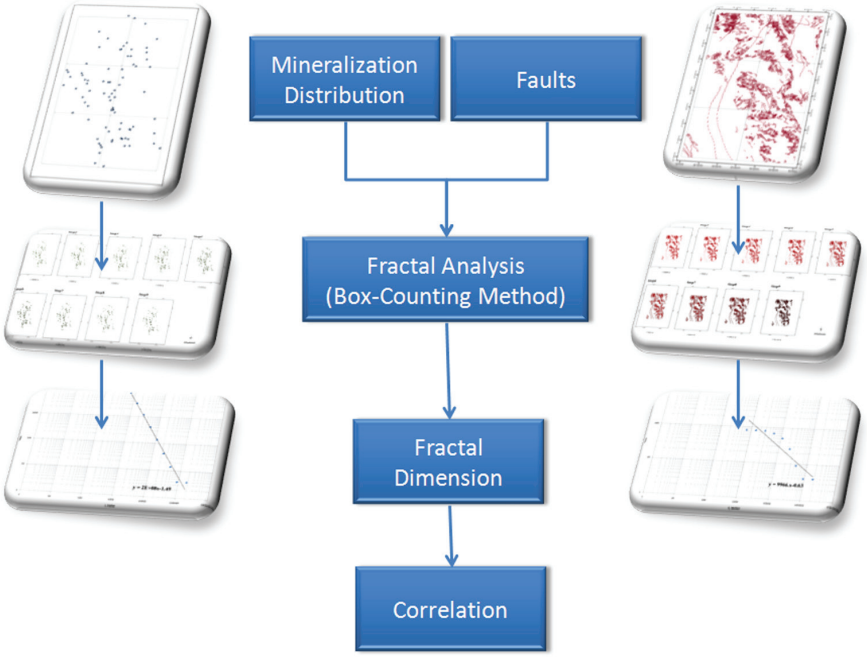

Figure 4. Schematic diagram showing the stagewise box-counting method fractal Analysis.

Table 3. Main trends of derivative rose diagrams from translation of mineralization points

ID	Class	Main trends
A	Total ore occurrence in whole of area	N-S
B	Ore indications in whole of area	N ،W ،NE
C	Mineral deposits and mines in whole of	NE-SW ،NE
D	Ore occurrence in north part of area	NE ،NW-SE ،W
E	Ore occurrence in south part of area	N ،W ،NE-SW،

Likewise, the fractal dimensions of faults and mineralization have been measured separately using the box-counting (Fig. 4) and number-in- circle methods (Fig. 5). The consequence of the processed data has been integrated as a separate layer with airborne geophysical data (Fig. 6).

Both the airborne magnetic data of the Geological Survey of Iran (GSI) obtained at 7.5 km line spacing and the more accurate data of the Atomic Energy Organization of Iran (AEOI) obtained at 500 m line spacing have been analyzed to determine the surface and deep magnetic anomalies. Appropriate filters have been applied to interpret airborne magnetic data (reduction to magnetic pole, first vertical derivative and upward continuation). All the aforementioned data have been spatially integrated to provide a better knowledge of the regional exploration assessment.

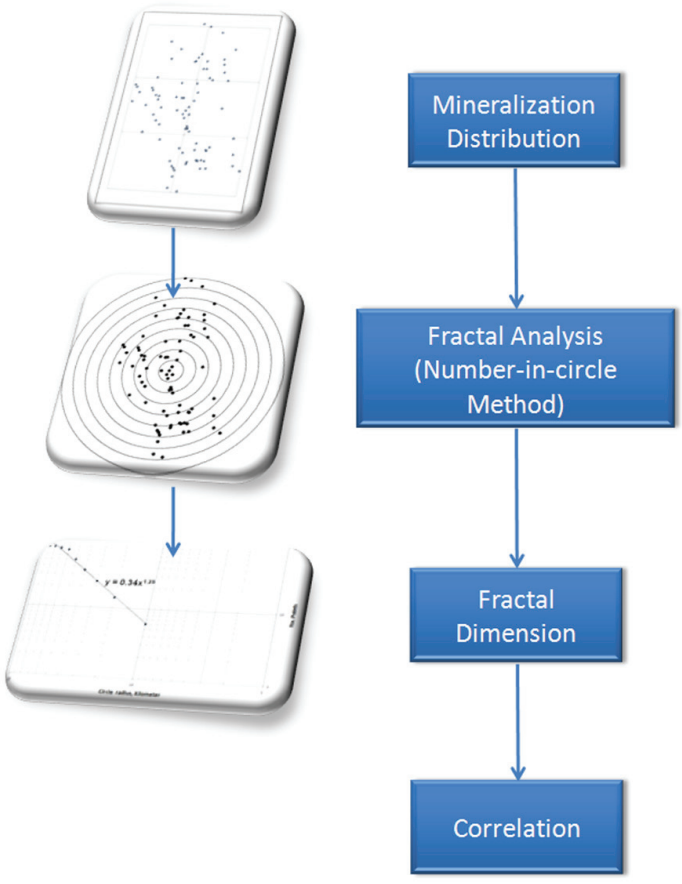

Figure 5. Schematic diagram showing the stagewise number-in-circle method Fractal Analysis.

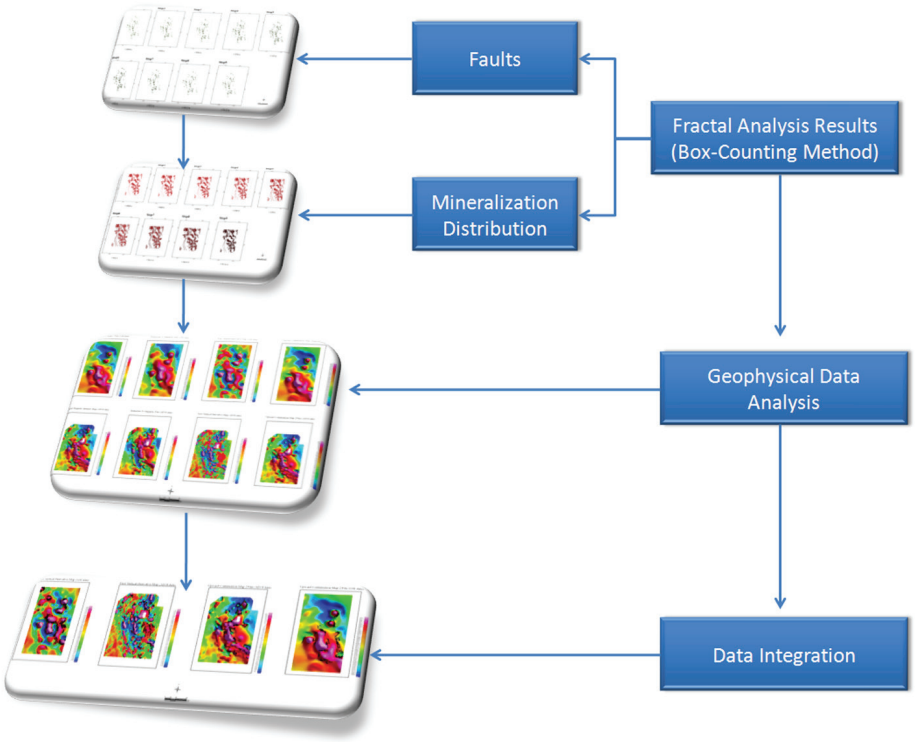

Figure 6. Schematic diagram showing the data integration procedure.

Fry Analysis

Fry analysis is a geometrical method used in directional studies. It employs spatial autocorrelation of points to assess distribution patterns of mineralization and potential controlling structures at the regional scale (Fry, 1979; Vearncombe & Vearncombe, 1999). Fry analysis for (n) data points, in this case mineral sites, will lead to (n (n-1)) translation points. Translation can be carried out both by manual and computer techniques (Vearncombe & Vearncombe, 1999). The manual technique involves two sheets of paper: one is the reference tracing paper on which the locations of main mineral site points are plotted along with the parallel reference vertical and horizontal lines, while the second is a transparent piece of paper that is marked by its center or origin point. The central point of the second sheet is placed on one mineral site in the first paper and all the other points are plotted on the second sheet and this procedure is repeated for every individual point in the first sheet. In this way, the assemblage of all translated mineral occurrence points, which can be referred to as reproduced points, allow us to study orientations in a set of mineral occurrence points.

The results of fry analysis (Tab. 3) show four prominent trends, namely N-S, W-E, NE-SW and NW-SE (Fig. 7).

Construction of rose diagrams of faults in individual quadrangles (Tab. 4) and in the whole study area (Fig. 8) helped to interpret the spatial patterns of the mineral deposits.

It can be deduced from the rose diagrams that four main trends are perpendicular to each other in pairs which correspond to the results of fry analysis. The aforementioned procedure confirms the structurally-controlled mineralization in the Bafq–Posht-e-Badam mining district that has been reported in earlier surveys (Haghipour, 1964; NISCO, 1969, 1971, 1974, 1975, 1979a, 1979b, 1980; Samani, 1988; Jami, 2005).

Other subsidiary trends are related to the younger fault generations and have no relationship to mineralization. Accordingly, measuring the fractal dimension of faults and occurrence patterns will reveal valuable exploration information.

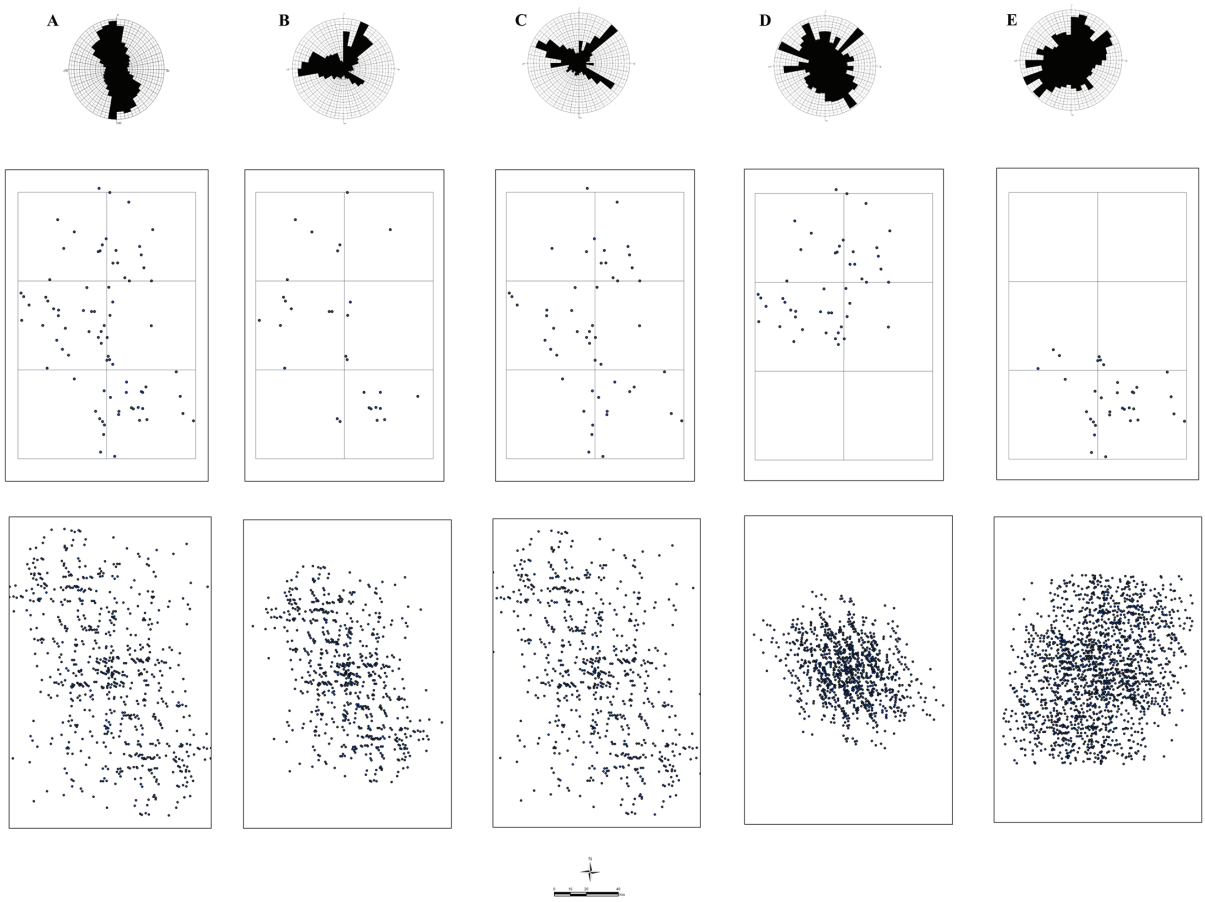

Figure 7. Rose diagrams showing ore occurrence distribution and translation points for: total ore occurrence, (A) ore indications, (B) mineral deposits and mines, (C) ore occurrence in the northern part of the area, (D) and ore occurrence in the southern part of the area, (E).

Table 4. Main trends of derivative rose diagrams from faults

ID	Quadrangle Name	Main trends
A	Zamanabad	NE-SW ,NW-SE
B	Saghand	NE-SW ,E
C	Chadormalou	N, NW
D	Ariz	SE ,S ,SW
E	Esfordi	N ,W ,NW-SE
F	Bafq	SE
G	All Sheets	N-S ,W-E,NE-SW,NW- SE

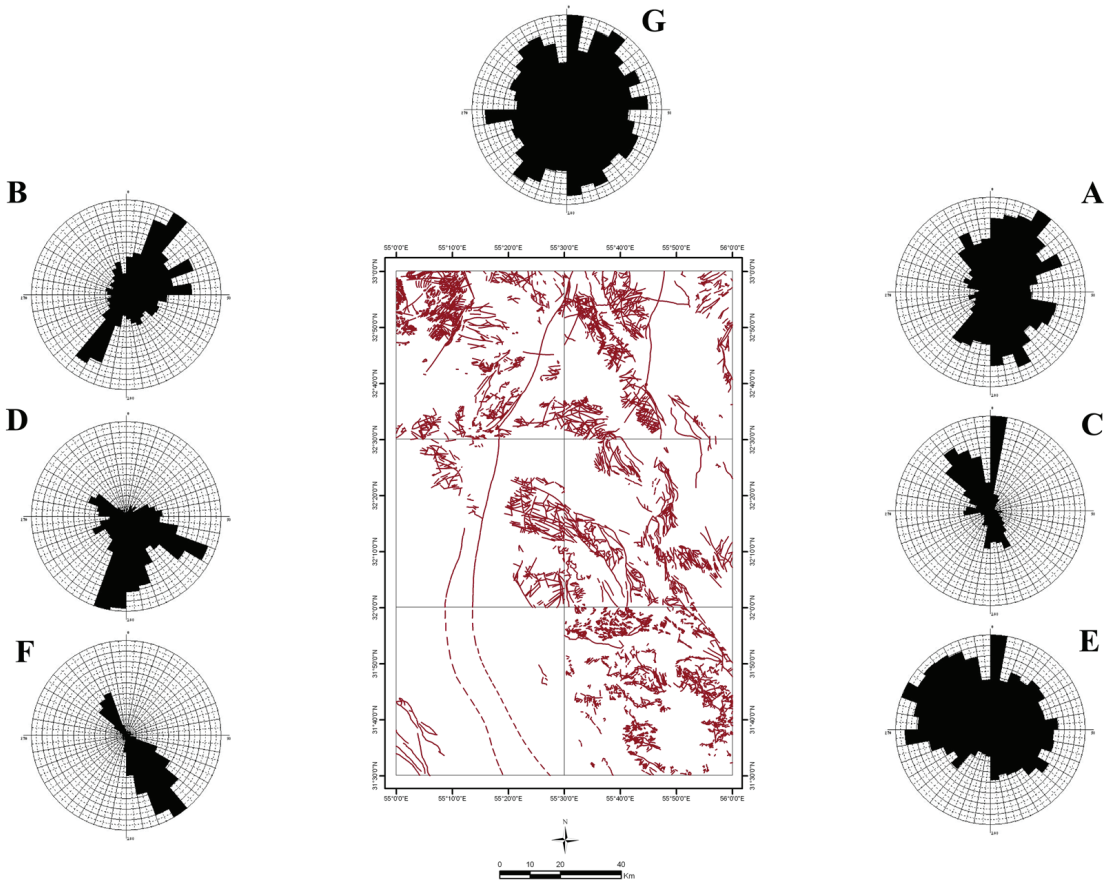

Figure 8. Rose diagrams for each quadrangle and total faults, based on 1:100000 scale geologic maps.

Fractal Analysis

Mandelbrot (1983) suggests that the distribution patterns of mineral occurrences in the earth may be fractals. Fractal geometry has been applied to analyze the spatial distribution of mineral occurrences (e.g. Blenkinsop, 1994; Agterberg *et al.,* 1996; Blenkinsop & Sanderson, 1999; Carranza, 2009). Fractal distributions may be measured by box-counting, density, number in-circle, fixed-mass, correlation or other methods; but since the box-counting method is more sensitive to the number of deposits, and will change with scale considerably (Blenkinsop, 1994), it is the most widely used method in which the number of squares containing the considered feature, N(r) of side (r), is measured as a function of (r). In the fractal relationship [$N(r) \alpha r^{-D}$], 'D' stands for the fractal dimension (Blenkinsop & Sanderson, 1999). In the number-in-circle method, a circle is drawn around the central point and the radius (r) is gradually increased. At each step, the total number of points N(r) inside the circle is counted. The slope of the best-fitting line to the logarithmic plot of N(r) versus (r) will provide the fractal dimension. Box-counting is also used to measure the fractal dimension of the fault pattern (Fig. 9).

At the first step, a 180000 m-side square is selected to conduct the study. Then the square is reduced repeatedly through 9 steps. During each step, all squares are divided into four smaller squares and counting is done in each step for the cells occupied by faults (Tab. 5).

To determine the fault fractal dimension D, a logarithmic graph of N(r) versus (r) is plotted in which N(r) is the number of cells (filled by faults) and (r) is the length of the square sides (Fig. 10), The straight line fitted best through the points satisfies the power-law relation (D =1.49).

Likewise, D is also measured for mineral occurrences by the box-counting method (Fig. 11), the result of which is reported in table 5.

A logarithmic graph of the number of cells filled by points versus the length of square sides is plotted to measure the D of points (Fig. 12).

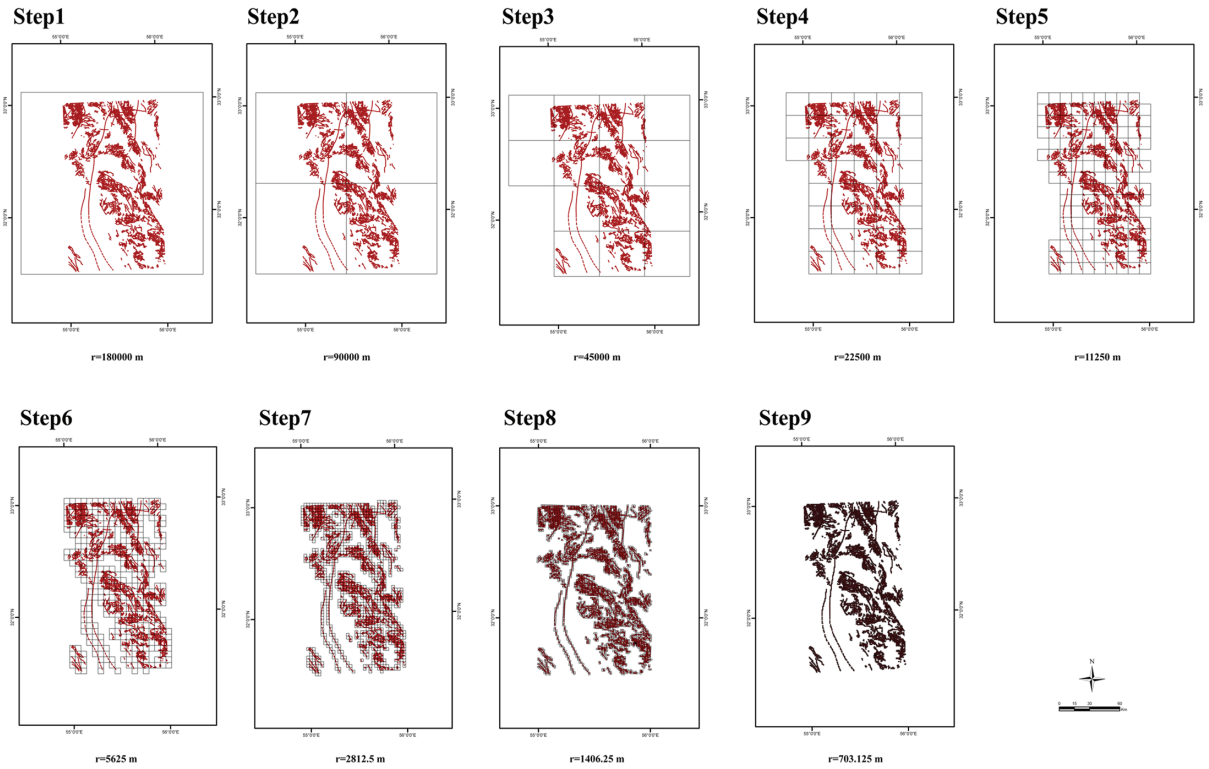

Figure 9. Stepwise presentation of box-counting method for measuring the fault fractal dimension D.

Table 5. Results of box-counting method for faults and occurrence points.

steps	Length of square sides	Total number of cells	Number of cells filled by occurrence points	Number of cells filled by faults
1	180000	1	1	1
2	90000	4	4	4
3	45000	16	9	14
4	22500	64	26	43
5	11250	256	51	138
6	5625	1024	69	416
7	2812.5	4096	80	1190
8	1406.25	16384	81	3324
9	703.125	65536	81	8956

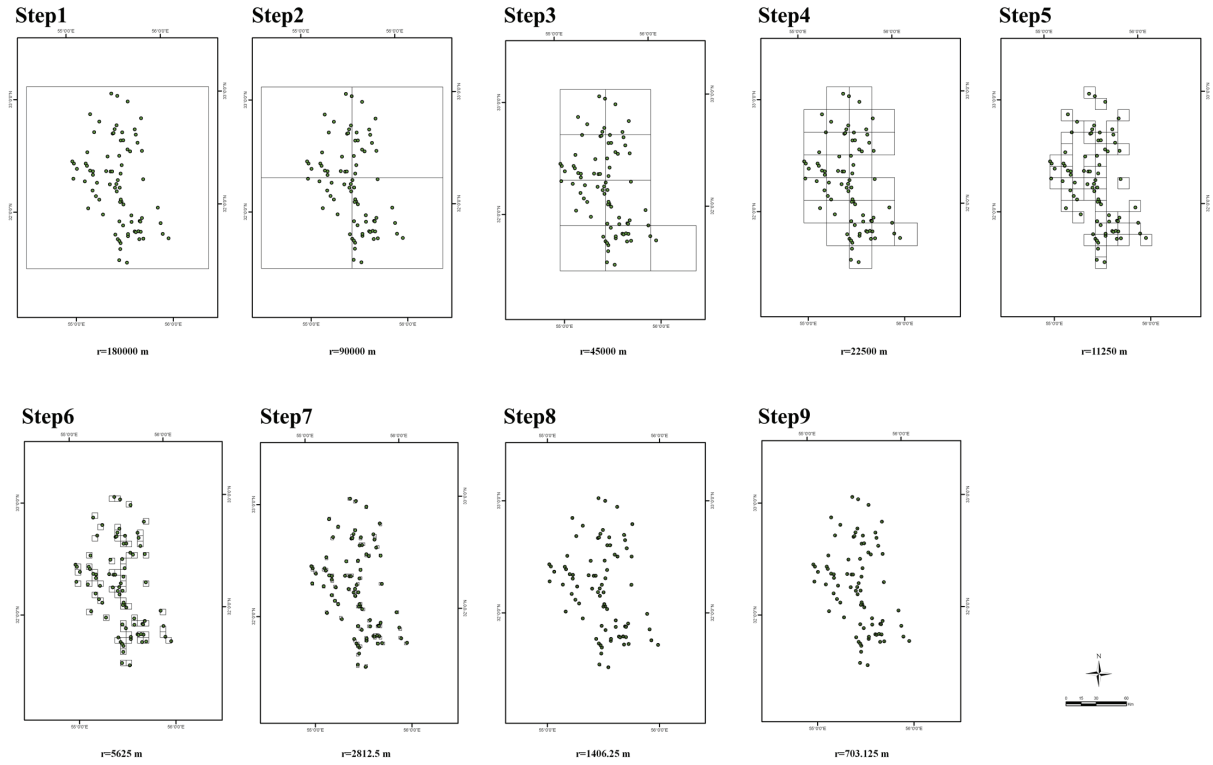

Figure 10. Logarithmic plot for number of cells filled by fault N(r) versus length of square sides (r, meter).

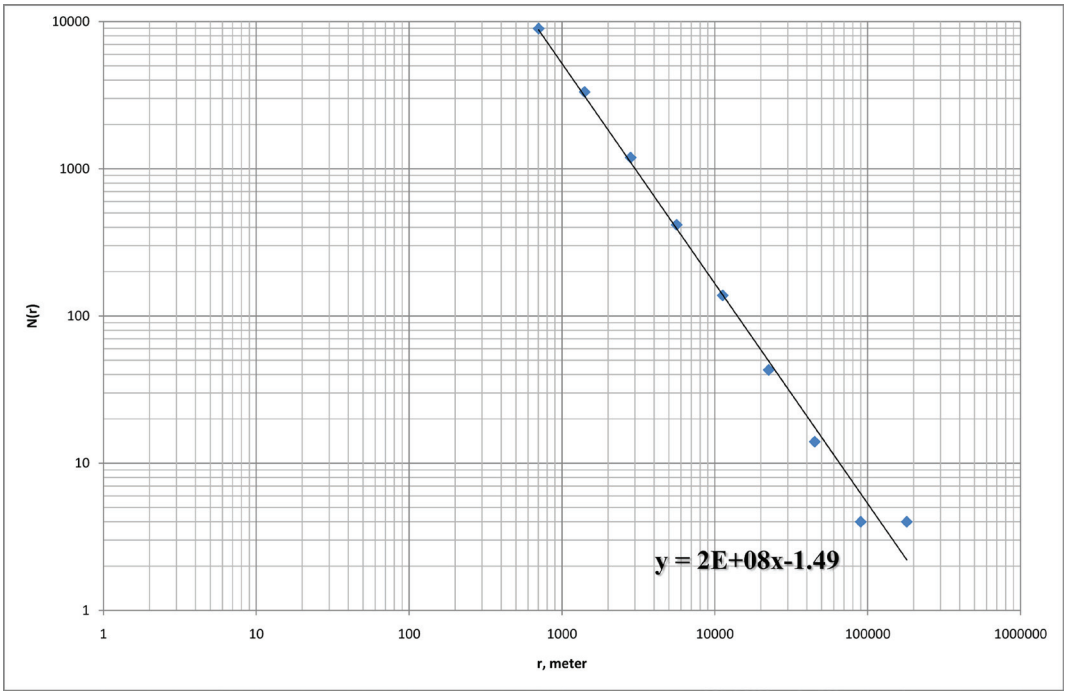

Figure 11. Stepwise presentation of the box-counting method for measuring fractal dimensions.

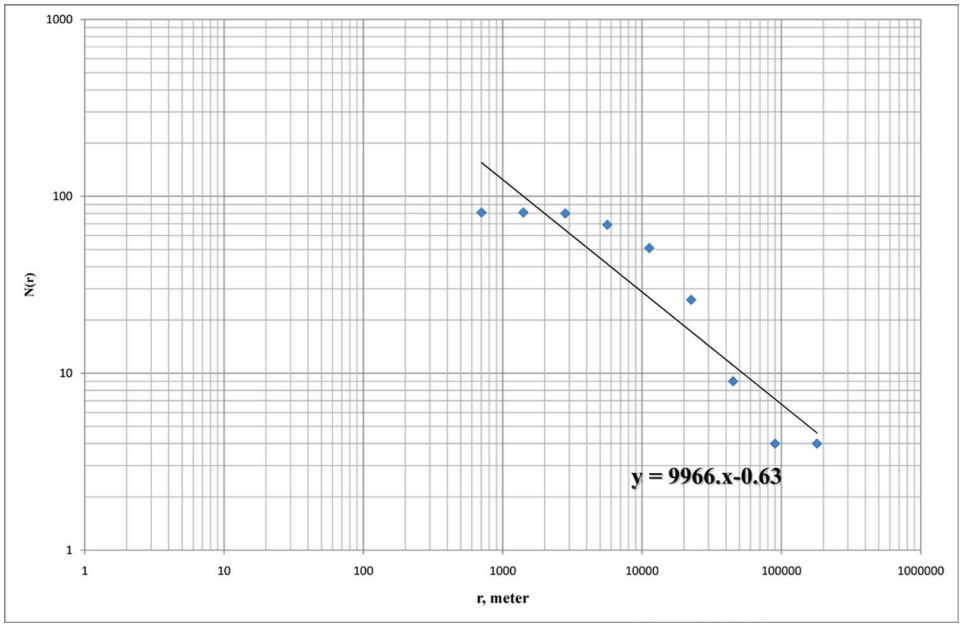

Figure 12. Logarithmic plot for number of cells filled by points N(r) versus length of square sides (r, meter).

The slope of the straight line fitted through the points shows D = 0.63 which is different from that of the faults. Perhaps the difference is due to the sensitivity of the box-counting method to small numbers of points. For this reason, the number-in-circle method is used to estimate the sensitivity of the box-counting method to the number of points (Fig. 13).

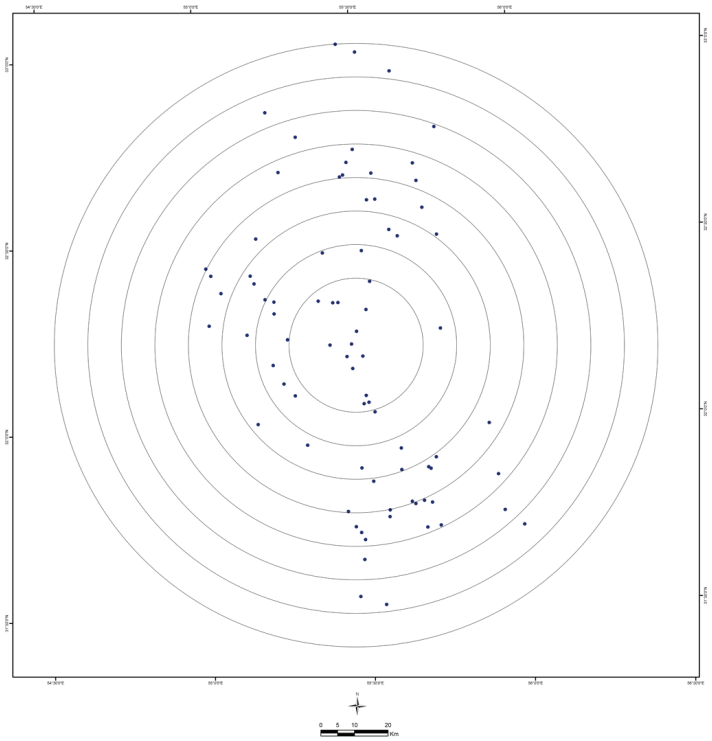

Figure 13. Number in circle method to measure fractal dimension of points.

The results of counting from 10 to 90 meter circles are presented in table 6. By plotting the logarithmic graph of counted points in each circle versus circle radius, D is measured to be 1.25 which is closer to the D of the faults by box-counting (Fig. 14).

Table 6. Results of number in circle method for faults and occurrence points.

Circles radius(Km)	Number of cells counted in circles
90	81
80	78
70	74
60	70
50	50
40	35
30	24
20	14
10	6

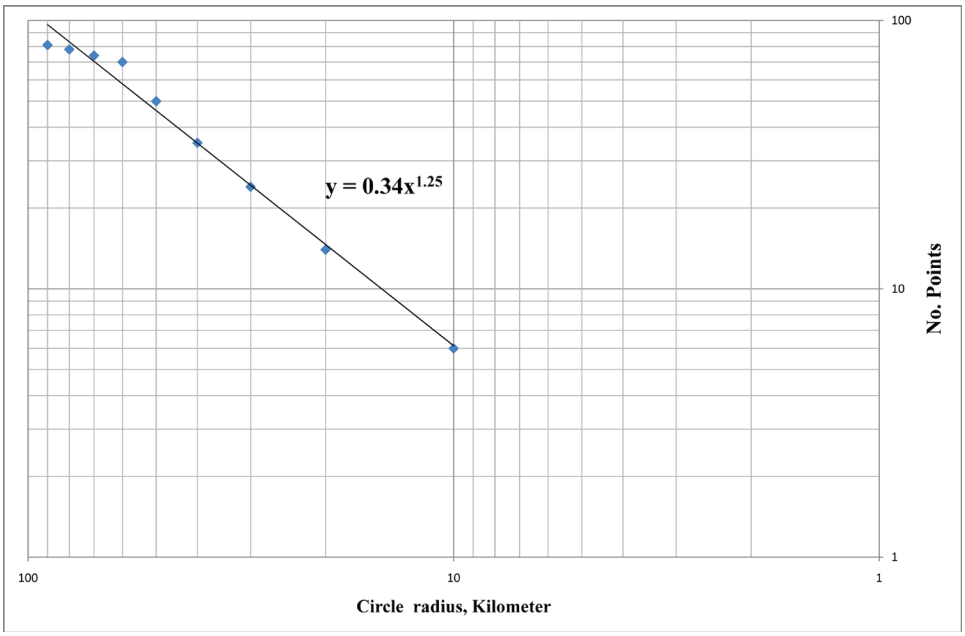

Figure 14. Logarithmic plot for number of cells filled by points N(r) versus circle radius (r, km)

Geophysical data integration

According to the field observations and the association between fault systems and mineralization confirmed by fry analysis, as well as the similarity between fractal dimension of faults and occurrence points, the sensibility and weakness of the box- counting method can be useful to define the exploration deficiency or the promising area for mineralization where we lack sufficient occurrence points. It may be used as an effective layer in GIS modeling. It should be noted that in different types of mineralization, other genetic factors are involved in the undiscovered mineral deposits which are not related to the weakness of the box- counting method. In order to reduce other genetic factors and select proper cells, geophysical data are used to demonstrate the promising cells which have magnetic anomalies as well as faults but lack any mineralization. Furthermore, many promising areas may indicate undiscovered mineralization at depth.

At the first step of geophysical data interpretation, the magnetic intensity map for the whole area is prepared. Consequently, the surface and deep anomalies are then defined using the required filters (Fig.15).

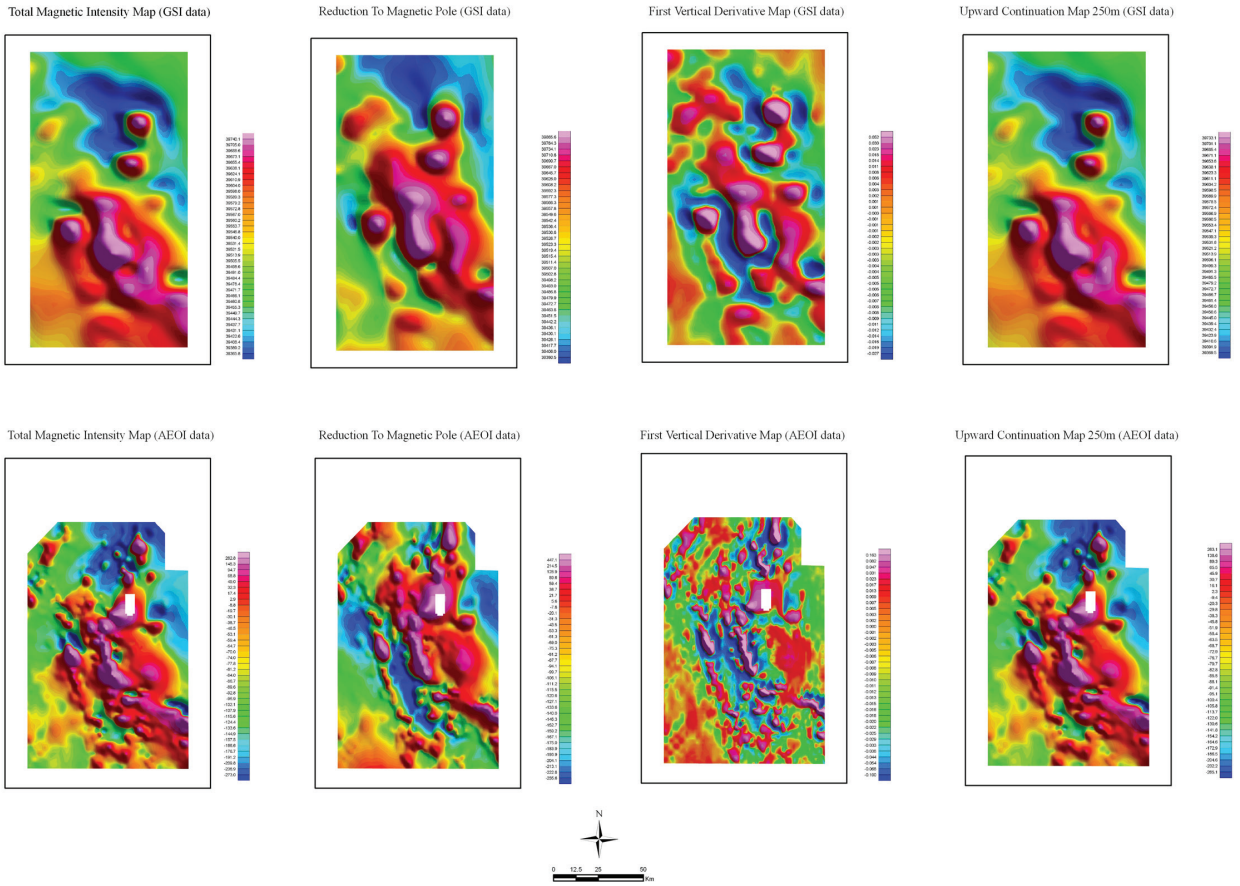

Figure 15. Geophysical maps resulting from indicated filters on GSI and AEOI data.

Pole reduction, first vertical derivative and upward continuation have all been used. The pole-reduction reconstructs the magnetic field of a data set as if it were at the pole. It means that the data can be viewed in a map-form with a vertical magnetic field inclination and declination of zero. In this way, the interpretation of the data is easier. The International Geomagnetic Reference Field (IGRF) model for the year 1975 has been used to measure the inclination and declination which are 48.55 and 2.55, respectively.

First vertical derivative was used to enhance the short wavelength component of the field and near-surface magnetic sources at the expense of deeper features (Fig.15). In addition to the first-vertical derivative, upward continuation was used to suppress the effect of shallow anomalies relative to the deeper sources. This is a low-pass filter, attenuating short-wavelengths more than long ones (Fig. 15).

Using the first vertical derivative map (for near-surface anomalies) and upward continuation map (for deeper anomalies) in combination, the iron anomalies can be revealed as high magnetic places near low magnetic areas. Based on the locations of known occurrences (Fig. 16), high magnetic anomalies adjacent to the low magnetic anomalies are the most suitable areas for iron exploration.

Fault-occupied cells have been defined during the measurement of fractal dimension for faults using the box-counting method. However, there are cells occupied by faults that do not match with cells occupied by mineral deposit occurrences that may be explained as follows:

1- No exploration activity has taken place yet in the no-match cells.
2- Some geologic and genetic parameters are involved that do not support structural factors in iron mineralization.

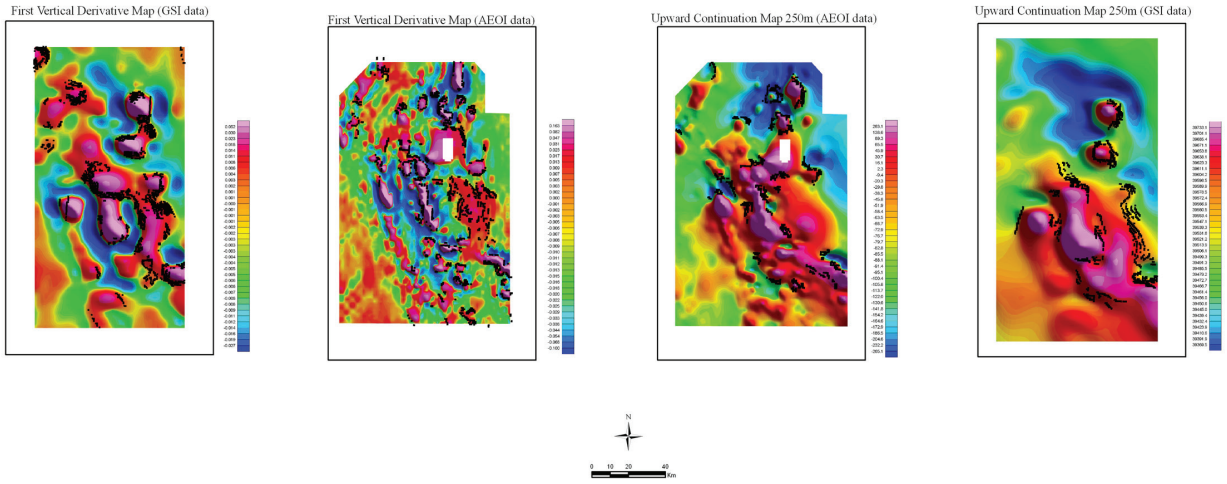

Figure 16. Spatial integration of fault-occupied cells (with no mineralization) and promising areas (black cells) determined from geophysical anomalies.

A question arises on the possibility of cells with both faults and magnetic anomalies, but no mineral occurrences.

Considering faults, geomagnetic anomalies and mineralization, the cells can be considered as occupied by faults and geomagnetic anomalies but without known occurrences and potential for further exploration. Magnetic anomalies strengthen the possibility and even alone, the existence of a magnetic anomaly indicates a magnetic body that most likely indicates an iron mineralization (Fig. 16).

Conclusion

Both fry and fractal analyses are spatial analytical methods that can be used to examine the spatial distribution of mineral deposit occurrences to support regional mineral exploration. In this study, we have analyzed the spatial distribution of 81 IOCG-type mineral occurrences and fault patterns in the Bafq–Posht-e-Badam Mining District using fry and fractal methods as regional exploration tools. Fry analysis of ore mineralization and faulting has confirmed the field observation of structurally-controlled ones. The fractal dimensions of ore mineralization and faults are 0.63 and 1.49, respectively. Because of the small number of ore mineralization points and the sensitivity of the box-counting method to the number of the data set points, it is supposed that the result does not seem close to reality; the figure 1.25 seems to be more realistic by the number-in-circle method. Indeed, we can turn the disadvantage or the weakness of box-counting method into an advantage. The geometrical investigation of mineral occurrence distribution pattern can lead us to understand the mineralization controlling factors using geo-statistical methods, especially fractal analysis.

Acknowledgments

The authors would like to thank M. Ehteshami, M. Kashefolhagh and M. Arafati (National Geoscience Database of Iran) for their review and constructive comments on the manuscript. This work was supported by the National Geoscience Database and the Geological Survey of Irán.

References

AGHANABATI, S.A. (2002): Major sedimentary structural units of Iran. Geological Survey of Irán.

AGTERBERG, F.P., CHENG, Q. & WRIGHT, D. F. (1996): Fractal modeling of mineral deposits. In: Elbrond, J. & Tang, X. Proceedings of the International Symposium on the Application of Computers and Operations Research in the Minerals Industries. Montreal, Canada, p. 43-53.

ALAVI, M. (1991): Sedimentary and structural characteristics of the Paleo-Tethys remnants in northeastern Iran. Geological Society of America Bulletin, **103**: 983-992.

AMINI, B., RASHIDI, H. & POSHTKOUHI, M. (2004): Geological Map of Bafq: Tehran, Geological Survey of Iran, scale 1:100 000.

BABAKHANI, A.R. & MAJIDI, J. (1995): Geological Map of Saghand: Tehran, Geological Survey of Iran, scale 1:100 000.

BABAKHANI, A.R. & GHALAMGHASH, J. (1999): Geological Map of Zamanabad: Tehran, Geological Survey of Iran, scale 1:100 000.

SOHEILI, M. & MAHDAVI, M.A. (1991): Geological Map of Esfordi: Tehran, Geological Survey of Iran, scale 1:100 000.

BARTON M.D. & JOHNSON D.A. (1996): Evaporitic source model for igneous-related Fe-oxide-(REE)-Cu-Au-U mineralization. Geology, **24**: 259-62.

BARTON M.D. & JOHNSON D.A. (2000): Alternative brine source for Fe-oxide (Cu-Au) systems: Implications for hydrothermal alteration and metals. In: TM Porter (ed), Hydrothermal iron oxide copper-gold and related deposits: A global perspective. PGC Publishing, Adelaide, 249 p.

BERBERIAN, M. & KING, G.C.P. (1981): Towards a paleogeographic and tectonic evolution of Iran. Canadian Journal of Earth Sciences, **18**: 210-265.

BIERLEIN, F.P., MURPHY, F.C., WEINBERG, R.F. & LEES, T. (2006): Distribution of orogenic gold deposits in relation to fault zones and gravity gradients: targeting tools applied to the Eastern Goldfields, Yilgarn Craton, Western Australia. Mineralium Deposita, **41**: 107-126.

BLENKINSOP, T. G. (1994): The fractal distribution of gold deposits. In: Kruhl, J. H. (ed.) Fractals and Dynamic Systems in Geosciences. Springer, Berlin, 247-258.

BLENKINSOP, T. G. & SANDERSON, D. J. (1999): Are gold in the crust fractals? A study of gold mines in the Zimbabwe craton. Fractures, fluid flow and mineralization. Geological Society of London, Special publications **155**: 141-151.

BONHAM-CARTER, G.F. (1994): Geographic information systems for geoscientists: modeling with GIS. Computer methods in the Geosciences. Pergamon, New York, 398 p.

BOOKSTROM, A.A. (1977): The magnetite deposits of El Romeral, Chile. Economic Geology, **72**: 1101-1130.

CARRANZA, E.J.M. (2009): Controls on mineral deposit occurrence inferred from analysis of their spatial pattern and spatial association with geological features. Ore Geology Reviews, **35**(3-4): 383-400.

DALIRAN, F. (1999): REE geochemistry of Bafg apatites, Iran: Implication for the genesis of Kiruna-type iron ores. Mineral deposits: Processes to processing, proceedings of the Fifth biennial SGA meeting and the Tenth quadrennial IAGOD symposium, London, Aug. 22-25, 1999, 631-634.

DALIRAN, F. (2002): Kiruna-type iron oxide-apatite ores and apatites of the Bafq district, Iran with an emphasis on the REE geochemistry of their apatites. In: TM Porter (ed), hydrothermal iron oxide copper-gold and related deposits: A global perspective. PGC Publishing, Adelaide, 377 p.

DALIRAN, F. & STOSCH, H. G. (2007): Multistage metasomatism and mineralization at hydrothermal Fe-oxide-REE-apatite deposits and "apatites" of the Bafq District, Central-East Iran. In: Stanely CJ *et al.* Digging Deeper, Proceedings 9th Biennial SGA Meeting Dublin 2007, 1501-1504.

EFTEKHARNEJAD, J. (1981): Tectonic division of Iran with respect to sedimentary basins. Journal of Iranian Petroleum Society, **82**: 19–28, (in Farsi).

FALCONER, K. (2003): Fractal Geometry. Mathematical Foundation and Applications, 2nd edition. Wiley, New York, 366 p.

FORSTER, H. & JAFARZADEH A. (1994): The Bafq mining district in Central Iran: A highly mineralized Infracambrian volcanic field. Economic Geology. **89**: 1697-1721.

FRIETSCH, R. (1978): The magmatic origin of the Kiruna-type. Economic Geology, **73**: 478-85.

FRY, N. (1979): Random point distributions and strain measurement in rocks. Tectonophysics, **60**: 89–105.

GHAEMI, F. & SAIDI, A. (2006): Geological Map of Chadormalou: Tehran, Geological Survey of Iran, scale 1:100 000.

GLEASON, J.D., MARIKOS, M.A., BARTON, M.D. & JOHNSON, D.A. (2000): Neodymium isotopic study of rare earth element sources and mobility in hydrothermal Fe oxide (Fe-P-REE) systems. Geochimica et Cosmochimica Acta, **64**: 1059-1068.

HAGHIPOUR, A. (1964): Iron ore deposits in Central Iran, in relation to structural geology and metamorphism, scapolitization and albitization. Journal of Iranian Petroleum Institute, **76**: 1-9.

HILDEBRAND, R.S. (1986): Kiruna-type deposits: their origin and relationship to intermediate subvolcanic plutons in the Great Bear Magmatic Zone, northwest Canada. Economic Geology, **81**: 640-659.

HITZMAN, M. W., ORESKES, N. & EINAUDI, M. T. (1992): Geological characteristics and tectonic setting of Proterozoic iron oxide (Cu-U-Au-REE) deposits. Precambrian Research **58**: 241-287.

HITZMAN, M.W. (2000): Iron oxide-Cu-Au deposits: what, where, when, and why. in: Hydrothermal Iron Oxide Copper-gold & Related Deposits: A Global Perspective (T.M. Porter, editor), 2, PGC Publishing, Adelaide, Australia, p. 9-25.

JAMI, M. (2005): Geology geochemistry and evolution of the Esfordi phosphate – Iron deposit, Bafq area, central Iran. MSc Thesis, the University of New South Wales, 384pp.

MAHDAVI, M. A. (1996): Geological Map of Ravar: Tehran, Geological Survey of Iran, scale 1:250 000.

MAJIDI, J. & BABAKHANI, A. R. (2000): Geological Map of Ariz: Tehran, Geological Survey of Iran, scale 1:100 000.

MANDELBROT, B. B. (1983): The Fractal behavior of nature. W. H. Freeman Company, New York, 483 p.

MARTIN, W., DIAZ, R., RUNEZ, R. & OLIVER, R. (1998): Calderon C and Calderon P. The undated Candelaria geologic mine model. Unpubl Rept.

NABAVI, M.H. (1972): Geological Map of Yazd: Tehran, Geological Survey of Iran, scale 1:250000.

NASLUND, H.R., HENRIQUEZ, F., NYSTROEM, J.O., VIVALLO, W. & DOBBS, F. M. (2002): Magmatic iron ores and associated mineralisation: Examples from the Chilean High Andes and Coastal Cordillera. In: TM Porter (Ed), hydrothermal iron oxide copper-gold and related deposits: A global perspective. PGC Publishing, Adelaide, PGC Publishing, Adelaide.

NISCO (1969): Report on the results of geological-geophysical prospecting for iron ores in the Bafq-Saghand area. Unpubl Rept. National Iranian Steel Corporation, Tehran. 195 p.

NISCO (1971): On the result of geological-geophysical prospecting for iron ores in the Bafq-Saghand and Zarand regions. Unpubl Rept. National Iranian Steel Corporation, Tehran. 195 p.

NISCO (1974): Material of geological prospecting work in the Bafq iron ore region for elaboration of a technical and economic report on iron ore prevision of the Esfahan steel plant in view of production expansion. Unpubl Rept. National Iranian Steel Corporation, Tehran. 81 p.

NISCO (1975): The results of the geological prospecting at the Chador Malu deposit. Unpubl Rept. National Iranian Steel Corporation, Tehran. 57 p.

NISCO (1979): Brief account on the Bafq iron ore region of Central Iran. Unpubl Rept. National Iranian Steel Corporation, Tehran. 149 p.

NISCO (1979): Detailed geological exploration carried out at the Chador Malu deposit. Unpubl Rept. National Iranian Steel Corporation, Tehran. 256 p.

NISCO (1980): Result of search and valuation works at magnetic anomalies of the Bafq iron ore region during 1976-1979, Unpublished Report, National Iranian Steel Corporation. 260 p.

NYSTROM, J.O. & HENRIQUEZ, F. (1994): Magmatic features of iron ores of the Kiruna-type in Chile and Sweden: Ore textures and magnetite geochemistry. Economic Geology **89**: 820-39.

RAMEZANI, J. & TUCKER, R.D. (2003): The Saghand region, Central Iran: U-Pb geochronology, petrogenesis and implications for Gondwana tectonics. American Journal of Science **303**: 622-665.

SAMANI B.A. (1988): Metallogeny of the Precambrian in Iran. Precambrian Research **39**: 85-106.

SILLITOE, R.H. & BURROWS, D.R. (2002): New field evidence bearing on the origin of the El Laco magnetite deposit, Northern Chile. Economic Geology **97**: 1101-1109.

TORAB, F.M. & LEHMANN, B. (2007): Magnetite-apatite deposits of the Bafq district, Central Iran: apatite geochemistry and monazite geochronology. Mineralogical Magazine **71**: 347-363.

VALEH, N. & HAGHIPOUR, A. (1970): Geological Map of Ardekan: Tehran, Geological Survey of Iran, scale 1:250 000.

VEARNCOMBE, J. & VEARNCOMBE, S. (1999): The spatial distribution of mineralization: Appllication of fry analysis. Economic Geology **94**: 475-486.